Renewable Energy, Environment, and Power Quality Journal (REE&PQJ)
ISSN:3020-531X
Volume 26, July 2026

Fast-Simulation Methods for LCC-S Wireless Power Transfer Systems in Electric Vehicles

Juan M. Perié[1], José F. Sanz[1], O. García-Izquierdo[1], Marta Calavia[1], Julio J. Melero[1] and M. Paz Comech[1]

[1] Instituto de Investigación Mixto de la Energía y la Eficiencia de los Recursos de Aragón, ENERGAIA
Universidad de Zaragoza-Fundación CIRCE
Mariano Esquillor 15, 50018 Zaragoza, Spain. +34976762402
jmperie@unizar.es, jfsanz@unizar.es, ogarcia@unizar.es, mcalavia@unizar.es, melero@unizar.es, mcomech@unizar.es

Abstract. The fast and iterative simulation of a large number of resonant power-electronics circuit cases is essential for optimizing control variables or for the optimal sizing of passive components in Wireless Power Transfer Systems. Commonly used approximations, such as the first-harmonic approximation, are useful for estimating certain electrical quantities, such as RMS current, phase or power, but they incur in significant errors in quantities that are more sensitive to distortion, such as switching current or peak values.
To achieve a suitable compromise between the simulation time required to analyse as many cases as possible and the accuracy of the resulting values, this work investigates the performance of three simulation methods: transient simulation, the first-harmonic approximation, and the Fourier-based approximation. In addition, the influence of simulation parameters, such as the transient simulation time or the number of harmonics considered, will be evaluated both in terms of computational cost and in the quality of the obtained results.

Key words. Resonant converters, wireless power transfer systems, EV wireless charging, steady-state simulation, multi-variable controllers.

1. Introduction

Resonant circuits in Power Electronics conversion stages offer significant advantages over traditional hard-switching technology [1], becoming the preferred choice in energy-conversion applications, as they enable:

1) *Higher switching frequency:* By allowing soft switching (ZVS or ZCS), they significantly reduce switching losses, which makes it possible to increase the operating frequency without incurring excessive losses associated with switching processes.
2) *More compact designs:* As the switching frequency increases, the amount of energy that must be stored in passive components such as inductors and capacitors decreases substantially. This reduction allows for smaller and more cost-effective equipment, as it also lowers the demand for raw materials.
3) *Reduced EMI:* Switching under ZVS or ZCS conditions results in lower dV/dt or dI/dt, respectively. This smooth transition of voltage or current generates fewer voltage spikes on DC buses and fewer abrupt variations in magnetic flux. Consequently, soft switching inherently eliminates EMC issues, avoiding the need for costly filters and shielding, as well as the technical risk of having to solve such problems at the end of the development cycle, when the prototype is already built and design flexibility is minimal.

In addition to offering these advantages, resonant circuits have been an enabling technology for several applications derived from high-frequency induction [2]. Clear examples include induction cooking and wireless power transfer [3]. This work will focus on the latter, specifically on wireless charging for Electric Vehicles.

Wireless charging for Electric Vehicles offers several advantages over conductive charging. It eliminates physical contact, avoiding mechanical wear and corrosion issues associated with plugs and connectors. It also enhances user convenience by enabling a fully automated charging experience in which the vehicle begins charging simply by being parked. In addition, it improves electrical safety by removing exposed energized parts and reducing the risk of sparks or moisture-related failures. Finally, it supports seamless integration in urban environments and enables advanced applications such as dynamic charging, where cable-based solutions would be impractical.

Such systems exhibit several characteristics that make them particularly complex:

1) *High parametric variability of the resonant electrical circuit.* The electrical parameters of the circuit depend on the type of vehicle coupled, its state of charge, the misalignment relative to the ground-side inductor, the vehicle's height depending on its load weight, and other factors. This becomes especially critical in dynamic

charging, where vehicle motion during charging process generates rapid and significant fluctuations in the self-inductance and mutual inductance values of the coupling elements.

2) *Advanced control requirements.* Due to the large parametric variation of the circuit, it is advisable to fully exploit all available control variables offered by the chosen Power Electronics topology. In traditional resonant systems, such as LLC converters, varying the switching frequency is generally sufficient to regulate power across the operating range. However, to operate optimally under any parametric variation of an inductive charging circuit, it is desirable to independently adjust the frequency, duty cycle, and phase shift of all half-bridges within the topology. Furthermore, the presence of distributed control, such as having part of the control system on the ground side and another part onboard the vehicle, without a shared low-latency interface, adds even more complexity to the operation and control of these topologies.

For all these reasons, the optimal design of resonant stages for wireless charging requires studying a large number of parametric variations within a very high-dimensional control-variable space, since many independent components are involved. Consequently, to design both the system components and the control strategy, it becomes necessary to run thousands of simulations to evaluate how the circuit operates under each combination of circuit parameters and control variables.

It is therefore essential to have a method for simulating resonant circuits that can compute their steady-state behavior as quickly as possible, while maintaining a good balance between computational cost and accuracy. Traditionally, this task has relied on costly transient simulations, to obtain highly accurate results for a limited number of cases, combined with first-harmonic approximations which, although fast enough to enable parametric sweeps of circuit and control variables, introduce significant errors in the voltage and current waveforms by assuming a purely sinusoidal approximation.

While this approach is useful in most scenarios, it forces designers to include large safety margins in ZVS and ZCS conditions to ensure that the harmonic distortion, present in reality but not captured in the model, does not momentarily violate soft-switching requirements. Such violations would generate very high-frequency transients, with their associated impact on EMC and with extreme heating and stress on components, which must internally dissipate the energy stored in the snubbers. In severe cases, this could even lead to irreversible damage to some electronic components.

For this reason, this article examines several fast-simulation approaches for resonant circuits, namely time-domain simulation, the first-harmonic approximation, and the Fourier-based approximation, evaluating the error introduced by each method as a function of its computational cost. The aim is to identify a suitable trade-off that enables control-scheme optimization without compromising robustness under any operating condition of the system.

2. Case Study

In order to analyze a case of sufficient complexity and real-world relevance, the wireless electric-vehicle charging system presented in [4] will be modeled.

The system consists of an LCC-S resonant circuit powered by a high-frequency full-bridge inverter, and its load is a diode rectifier bridge followed by a DC-DC converter placed between the rectifier and the vehicle's battery.

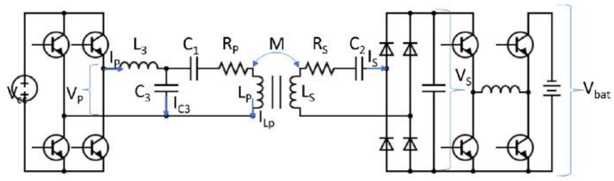

Fig. 1. Electronic model of the WPT.

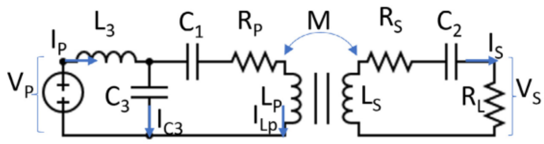

Fig. 2. Simplified model.

To enable a fair comparison of the system's operating point across all methods, a single case will be analyzed, defined by a specific relative positioning between the primary and secondary inductors, the DC voltage levels, and the control variables. These parameters are presented in Table I.

Table I. – Circuit parameters.

PARAMETER	VALUE
C_1	$37.89\ nF$
C_2	$19.83\ nF$
C_3	$70.57\ nF$
L_1	$136.41\ \mu H$
L_2	$190.1\ \mu H$
L_3	$49.56\ \mu H$
R_1	$177.96\ \Omega$
R_2	$323.05\ \Omega$
M_{12}	$50.13\ \mu H$
V_{CC}	$800\ V$
V_{bat}	$778{,}8\ V$
f_{sw}	$85\ kHz$

The accuracy of the models and simulation methods can be validated using the experimental tests conducted in Fig. 3. These tests provide the actual voltage and current waveforms, which are presented in [4].

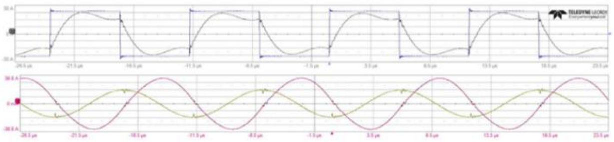

Fig. 3. Waveform obtained with the oscilloscope in Position 1 of [4]: Vp (blue), Ip (gray), ILp (yellow) and Is (pink).

3. Steady-state Simulation

Due to the high switching frequency of resonant circuits, the frequency separation between the fundamental harmonic of the electrical circuit and the bandwidth of the control feedback loop is sufficiently large to assume that no interaction occurs between them. Consequently, the transient evolution of the resonant circuit does not influence the control mode, allowing the controlled plant to be considered as a system without dynamics, whose response is purely static and depends solely on its steady-state operating conditions. Therefore, the objective is to determine the circuit behaviour under these steady-state conditions.

3.1 Transient simulation

To provide a reference for assessing the error introduced in the various approximations, without considering the modelling error relative to the experimental results, a full simulation of the circuit will be carried out, encompassing both its transient and steady-state regimes. The electrical circuit must be expressed in the form shown in (1).

$$\dot{X} = AX + BU \tag{1}$$

From the differential equations that model the circuit, a state-space representation can be derived, defined by the state variables and inputs shown in (2), and characterized by the matrices A and B presented in (3) and (4).

$$X = \begin{pmatrix} I_P \\ V_{C_3} \\ I_{LP} \\ V_{C_1} \\ I_S \\ V_{C_2} \end{pmatrix}; \quad U = \begin{pmatrix} V_P \\ V_S \end{pmatrix} \tag{2}$$

$$A = \begin{pmatrix} 0 & -1/L_3 & 0 & 0 & 0 & 0 \\ 1/C_3 & 0 & -1/C_3 & 0 & 0 & 0 \\ 0 & KL_S & -KL_SR_P & -KL_S & -KMR_2 & -KM \\ 0 & 0 & 1/C_1 & 0 & 0 & 0 \\ 0 & KM & -KMR_P & -KM & -KL_PR_2 & -KL_P \\ 0 & 0 & 0 & 0 & 1/C_2 & 0 \end{pmatrix} \tag{3}$$

$$B = \begin{pmatrix} 1/L_3 & 0 \\ 0 & 0 \\ 0 & -KM \\ 0 & 0 \\ 0 & -KL_P \\ 0 & 0 \end{pmatrix} \tag{4}$$

$$K = \frac{1}{L_PL_S - M^2} \tag{5}$$

Using the backward Euler method, the evolution of the state variables can be computed from the inputs by iteratively evaluating expression (6).

$$X_K = (I - T_S \cdot A)^{-1} \cdot X_{K-1} + (I - T_S \cdot A)^{-1} \cdot T_S \cdot B \cdot U_K \tag{6}$$

Consequently, it only remains to define the values of U_k corresponding to the inverter and load-rectifier voltages. The inverter voltage is obtained from the inverter PWM control parameters and the DC-bus voltage, whereas the input voltage of the rectifier depends on the direction of the secondary current, following law (7).

$$V_S = \begin{cases} I_S > 0 \Rightarrow V_{bat} \\ I_S < 0 \Rightarrow -V_{bat} \end{cases} \tag{7}$$

By iteratively computing this model over the simulation time domain, the transient current evolution in all elements is obtained. Fig. 4 shows the inverter voltage and current at the beginning of the transient simulation, which exhibit a damped response, as illustrated in Fig. 5, eventually reaching a periodic steady-state response such as that shown in Fig. 6.

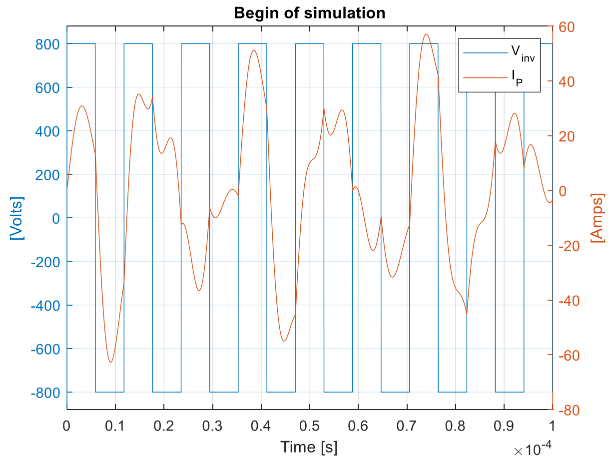

Fig. 4. Voltage and current throught the inverter at the beginning of simulation.

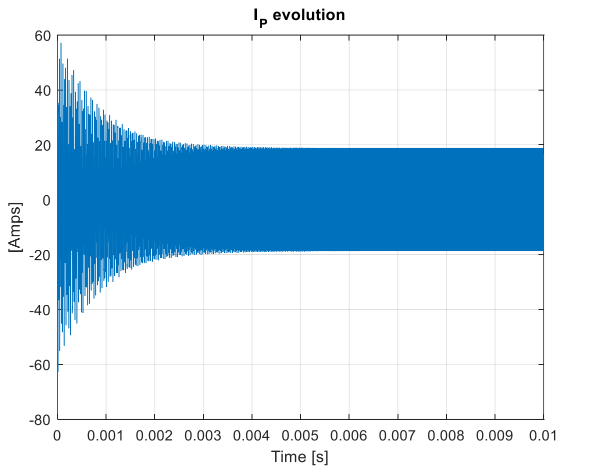

Fig. 5. Transient evolution of the inverter current until the steady-state is reached.

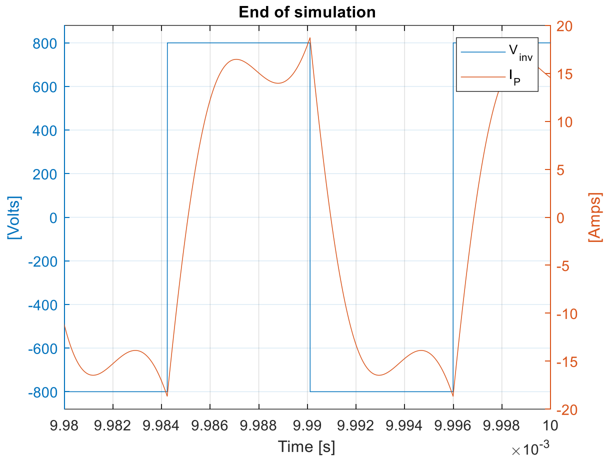

Fig. 6. Steady-state inverter current.

As can be observed, the inverter current steady-state response (Fig. 6) closely matches that obtained with the actual system, as measured in the experimental tests shown in Fig. 3. The output rectifier waveform is also consistent with the expected behavior of a full-bridge rectifier (Fig. 7).

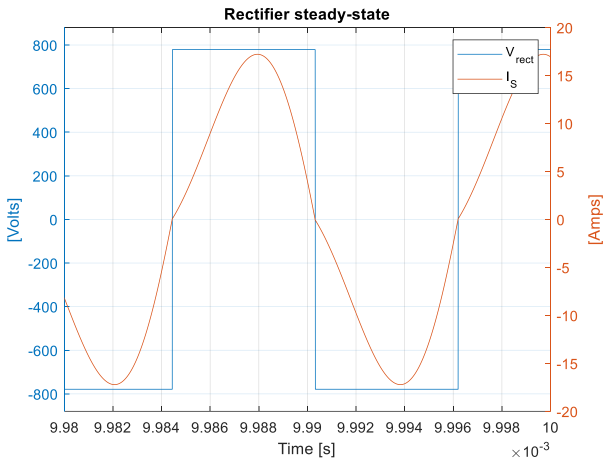

Fig. 7. Steady-state rectifier voltage and current.

3.2 First-Harmonic Approximation

The most used approximation in circuit analysis and design, due to its simplicity, is the first-harmonic approximation. This approach relies on the fact that, in a resonant system with a sufficiently high quality-factor, the electrical circuit behaves as a highly selective filter around the resonant frequency, making the influence of harmonics other than the fundamental negligible. Consequently, only the first-harmonic component of the inverter-injected voltage is considered, as given by (8).

$$(V_1)_{RMS} = \frac{2\sqrt{2}}{\pi} \mathrm{V_{cc}} \tag{8}$$

On the other hand, the secondary-side rectifier can be approximated as a linear resistance. This follows from the fact that, if the current waveform is close to a pure sinusoid, the first harmonic of the rectifier's square-wave voltage will be in phase with the current it rectifies. The value of this equivalent resistance can be determined from the desired output power, which is assumed to be regulated. Accordingly, its value may be imposed based on the power delivered to the load, as expressed in equation (9).

$$R_L \approx \frac{8}{\pi^2} \cdot \left(\frac{\mathrm{V_S^2}}{\mathrm{P_D}}\right) \tag{9}$$

With this approximation, the first-harmonic response of the circuit in Fig. 2 can be computed using the phasor equations corresponding to its sinusoidal steady-state model.

The simulation results obtained with this approximation are shown in Fig. 8 for the inverter current and in Fig. 9 for the rectifier current. As can be observed, the approximation is adequate for evaluating quantities such as power and RMS current, but it is less accurate for assessing other converter design parameters, such as the instantaneous current at the switching instant, which is significantly underestimated, as illustrated in Fig. 8.

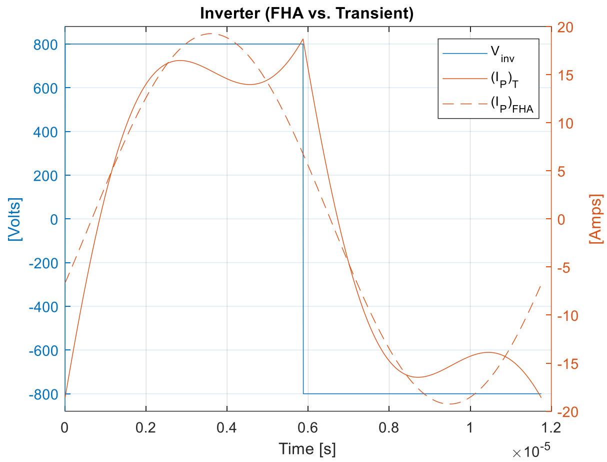

Fig. 8. First Harmonic approximation vs. transient simulation of inverter current.

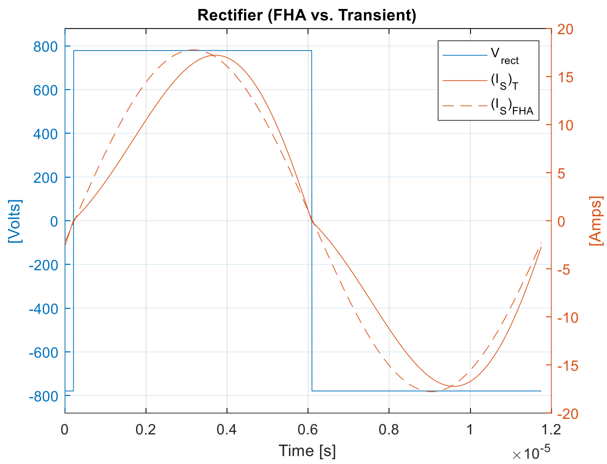

Fig. 9. First harmonic approximation vs. transient simulation of rectifier current.

3.3 Fourier Approximation

Any periodic function can be decomposed into a superposition of sinusoidal waves whose frequencies are integer multiples of the fundamental, which corresponds to the excitation frequency. This allows the circuit's behaviour to be analysed for all harmonics, since the waveforms can be approximated as the sum of the individual harmonic responses. In principle, this yields the complete steady-state response, including distortion.

However, this approach presents a challenge in modeling the rectifier bridge, since it is a nonlinear element. The equivalent resistance model (9) is only valid for the fundamental harmonic, and it is not possible to determine a priori the equivalent resistance that the rectifier exhibits for each harmonic.

To address this issue, the characteristics of resonant circuits, and especially of the LCC-S topology, have been considered. As shown in Fig. 9, the harmonic components of the current do not significantly contribute to the zero-crossing phase shift, since the current waveform is largely dominated by the fundamental harmonic. Moreover, given that the characteristic voltage waveform at the rectifier is a square wave synchronized with the zero-crossing, the phasor values of each harmonic of the rectifier input voltage can be established, following the decomposition expressed in (10).

$$(\overline{V}_2)_h = \left(\frac{2\sqrt{2}}{h \cdot \pi} V_{DC2}\right)_{h\cdot(\angle I_2)_{h=1}} \tag{10}$$

Knowing the phasor of the voltage $(\overline{V}_2)_{h=1}$ obtained from the first-harmonic approximation, the magnitude and phase of each harmonic can be determined using (11), which follows from (10).

$$(\overline{V}_S)_h \approx \left(\frac{(V_S)_{h=1}}{h}\right)_{h\cdot\angle(I_2)_{h=1}} \tag{11}$$

Consequently, the response to the higher-order harmonics can be computed by applying the Superposition Principle. First, the contribution of the inverter-voltage harmonics $(V_P)_h$, which are known a priori, will be considered in the circuit of Fig. 2, while setting $(V_S)_{h=0}$. Subsequently, by considering the case in which $(V_P)_h = 0$ and using the values of $(V_S)_h$ calculated according to expression (11), a good approximation of the full harmonic response of the circuit can be obtained, as shown in Fig. 10 and Fig. 11.

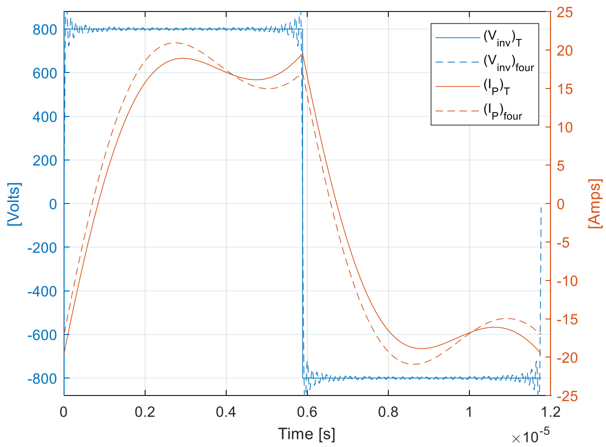

Fig. 10. Fourier approximation of inverter current.

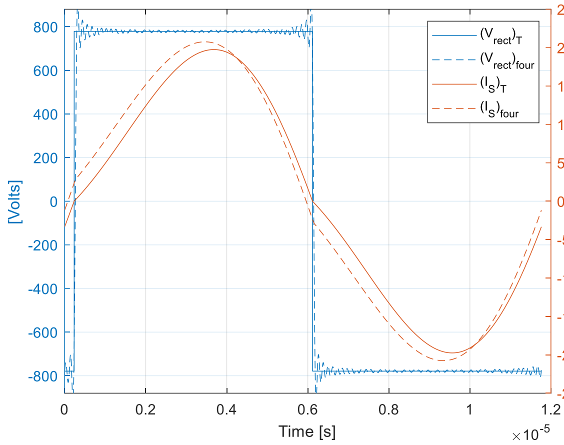

Fig. 11. Fourier approximation of rectifier current.

4. Results

Using these approximations, a batch of tests of the simulation methods described above has been carried out. A sweep of different parameterizations has also been performed, such as the number of harmonics (in log-spaced sweep from $h = 3$ to $h = 1{,}000$) in the Fourier-based method or the simulation time (log-spaced from $T = 100\mu s$ to $T = 100ms$) in the transient method.

From the tests conducted, both the execution time required to perform the simulation and the Relative Error of the various design quantities of interest (such as the RMS currents through the inductive components, the switching currents, and the load power) have been compared.

As shown in Fig. 12, the approximate methods, even the first-harmonic approach, provide a good estimation of the RMS values in the ground-side circuit, although they exhibit larger errors in determining the secondary RMS current and the load power. The poorest results arise in the low-order harmonic approximations of the switching current, a critical quantity for the thermal design of the inverter or for the development of more advanced control strategies. Traditionally, this limitation has been addressed by adopting generous safety margins, which penalize efficiency.

All relative errors decrease as the number of harmonics included in the model increases, except for the quantities related to the secondary current and the rectifier power. In these cases, the phase-approximation error of each rectifier-voltage harmonic cannot be compensated.

It can also be concluded that there is no practical benefit in performing a Fourier-based simulation with more than 50 to 100 harmonics, since the resulting error does not improve, whereas the computational cost increases proportionally with the number of harmonics.

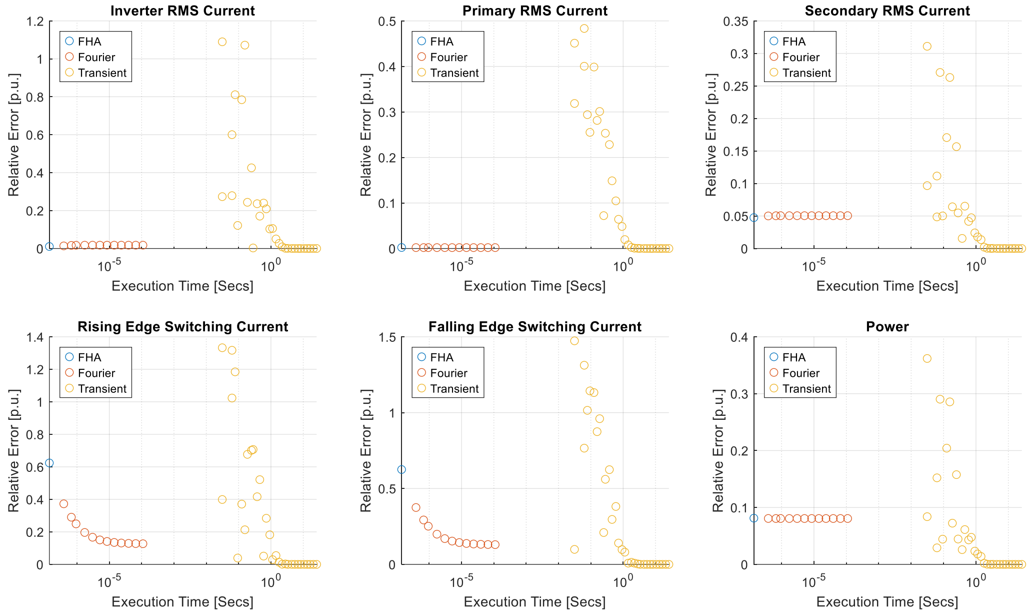

Fig. 12. Relative error of each design variable as a function of the simulation method and the execution time required.

On the other hand, the transient analysis exhibits excellent accuracy, both in the ground-side and on-board circuits, but at the cost of an execution time several orders of magnitude higher than that of the approximate methods. When the simulation time is reduced, the resulting values show no meaningful correspondence with the expected behavior. Altogether, this makes transient analysis unsuitable for optimization procedures that require a massive number of simulations, such as Pareto optimization methods.

5. Conclusion

The results obtained confirm that the only feasible method for designing this type of system through parameter-sweep techniques is to rely on approximate models, such as the commonly used first-harmonic approximation, while reserving the more accurate methods for validation at a limited number of operating points of particular interest, carried out after the design process.

Furthermore, a gap of several orders of magnitude has been observed between the execution time of the approximate models and that of the transient simulation. Within this gap lies the opportunity to develop new simulation methods that strike a balance between execution time and model accuracy. This represents a promising research direction that could accelerate the optimal design of resonant systems and enable the practical implementation of more complex converters or more sophisticated control strategies.

Acknowledgement

This paper is part of the R&D+i project PID2022-141796OB-I00 DISEÑO OPTIMO DE BOBINAS INDUCTORAS PARA SISTEMAS DE CARGA DE VEHICULOS ELECTRICOS MULTIMODAL funded by MCIN/AEI/10.13039/501100011033 and by ‘‘ERDF A way of making Europe’’.

References

[1] R. L. Steigerwald, “A Comparison Of Half-Bridge Resonant Converter Topologies,” *IEEE Trans. Power Electron.*, vol. 3, no. 2, pp. 174–182, 1988, doi: 10.1109/63.4347.

[2] S. Y. R. Hui, W. Zhong, and C. K. Lee, “A critical review of recent progress in mid-range wireless power transfer,” *IEEE Trans. Power Electron.*, vol. 29, no. 9, pp. 4500–4511, 2014, doi: 10.1109/TPEL.2013.2249670.

[3] J. Sallán, J. L. Villa, A. Llombart, and J. F. Sanz, “Optimal design of ICPT systems applied to electric vehicle battery charge,” *IEEE Transactions on Industrial Electronics*, vol. 56, no. 6, pp. 2140–2149, 2009, doi: 10.1109/TIE.2009.2015359.

[4] O. García-Izquierdo, J. F. Sanz, J. L. Villa, and G. Martin-Segura, “Optimal design of an LCC-S WPT3 Z1 SAE J2954 compliant system, using NSGA-II with nested genetic algorithms for simultaneous local optimization,” *Appl. Energy*, vol. 367, no. 6, p. 123369, Aug. 2024, doi: 10.1016/j.apenergy.2024.123369.

[5] R. Bosshard and J. W. Kolar, “Multi-Objective Optimization of 50 kW/85 kHz IPT System for Public Transport,” *IEEE J. Emerg. Sel. Top. Power Electron.*, vol. 4, no. 4, pp. 1370–1382, Dec. 2016, doi: 10.1109/JESTPE.2016.2598755.